# Magnetic anisotropy of glide-distorted fcc and of bcc ultrathin Fe/Cu(001) films

D. E. Fowler and J. V. Barth
*IBM Research Division, Almaden Research Center, 650 Harry Road, San Jose, California 95120*
(Received 7 August 1995)

The effective anisotropy fields, $H_{\text{eff}}$, of Fe films of 2 to 15 monolayers thick grown on Cu(001) were measured at 100 K for two growth conditions; 100 K growth with a room temperature anneal and room-temperature growth. First-order anisotropy constants, $K_v$ and $K_s$, are derived for the thickness independent anisotropy energy term and the thickness dependent anisotropy energy term, respectively. For 100 K growth, $K_v$ for the glide-distorted fcc Fe film is two orders of magnitude larger than for the bcc Fe film and $>30$ times larger than for bulk bcc Fe. The fcc film has $K_s=0.26$ ergs/cm$^2$, compared to 0.94 ergs/cm$^2$ for the bcc Fe film. The perpendicular easy axis in the glide-distorted fcc Fe, for either growth temperature, is observed only because both $K_v$ and $K_s$ result in large perpendicular anisotropy energies. A conversion to an in-plane easy axis occurs as the thickness dependent anisotropy energy decreases with increasing Fe thickness in the bcc phase and is not directly a result of the phase transformation to bcc Fe. Room-temperature growth gives similar anisotropy constants.

## I. INTRODUCTION

The desire to grow ferromagnetic, fcc Fe has stimulated a tremendous number of experimental studies of Fe growth on Cu(001). The complex atomic structure of ultrathin fcc Fe films,[1–4] the variations observed with growth conditions,[5] and the variety of magnetic states in these films[5,6] has made clarification of the origin of the ferromagnetism and its relationship to atomic structure an extremely demanding challenge. Only recently has the atomic structure been determined in enough detail to show that the ferromagnetism in fcc Fe films is directly related to a glide reconstruction of the fcc Fe along $\langle 110\rangle$ directions.[2,4,5] These distortions of the lattice are similar, although of smaller magnitude, to the atomic shear which occurs during the martensitic fcc-bcc phase transformation at higher Fe coverages.[7] An unreconstructed Fe fcc lattice does not form on the Cu(001) substrate for low-temperature growth. For room-temperature (RT) growth, fcc Fe does form for Fe coverages between 5 and $\sim 9$ monolayers (ML), but even these Fe films have a $\langle 110\rangle$ glide reconstruction at the surface. Concurrent with the glide distortions are atom layer expansions normal to the film of about 6% in each glide-distorted layer. Additionally, the glide-distorted fcc Fe layers are nonpseudomorphic with the Cu(001) substrate,[4,8] although there may still be residual strain as indicated by the atomic disorder observed in the Cu.[4] An explanation of the observed ferromagnetism in fcc Fe consistent with theory[9] is that it is associated with the increased atomic volume of the Fe participating in the glide distortion relative to perfect fcc Fe.

In addition to the magnetic moment and the magnetic coupling state, the magnetic anisotropy is a fundamental property of all magnetic materials. The easy axis of magnetization in Fe/Cu(001) films was one of the first magnetic properties to be measured for these films.[10] However, a quantitative evaluation of the anisotropy energies and the relationship of the anisotropy to atomic structure has not been fully explored. The anisotropy can be quantified from analysis of the total energy of a magnetic film in an external applied field, $H$, assuming uniaxial anisotropy, according to

$$E=\text{const}+[2\pi M_s^2-K_1]\sin^2\theta+K_2\sin^4\theta-M_sH\cos(\alpha-\theta), \tag{1}$$

where $2\pi M_s^2$ is the shape anisotropy in the thin-film limit, $M_s$ is the saturation magnetization, $K_1$ is the first-order anisotropy constant, $K_2$ is the second-order anisotropy constant, $\theta$ is the angle between the easy axis and $M_s$, and $\alpha$ is the angle between $H$ and the easy axis. The last term in Eq. (1) is the magnetic potential energy or Zeeman energy. Minimization of the total energy with respect to $\theta$ results in an expression for the effective anisotropy field, a measurable quantity:

$$H_{\text{eff}}=4\pi M_s-\frac{2K_1}{M_s}. \tag{2}$$

For ultrathin-film studies, $K_1$ is often redefined as a combination of a constant for the thickness-independent anisotropy, $K_v$, often called the volume anisotropy constant, and a constant for the thickness-dependent anisotropy, $K_s$, often called the surface-interface anisotropy constant, according to

$$K_1=K_v+\frac{2K_s}{t}, \tag{3}$$

where $t$ is the thickness of the magnetic film. The atomic structure of the magnetic film has a large influence on both $K_v$ and $K_s$ through crystalline anisotropies, internal film strain, and the formation of interfaces or a surface. As recently discussed for Ni on Cu(001),[11] lattice strain in the magnetic film due to epitaxy or to reconstructions can be important in determining the easy axis of magnetization. At the same time a breakdown of pseudomorphic growth, above some critical thickness, will gradually release the lattice strain with increasing thickness through the formation of dislocations or other lattice defects. This can lead to a thickness-dependent anisotropy that has its origin in the volume of the film rather than the surface.[12] Until the atomic

 

structure of a magnetic thin film is known, it is very difficult to obtain good values of the anisotropy constants and to proceed to the next step of rationalizing the magnitude of these constants.

The objective of this paper is to present a determination of the anisotropy constants for Fe films grown on Cu(001) using magneto-optic Kerr effect (MOKE) techniques and to put these results in the context of the newly determined atomic structures of the Fe films. We first describe the experimental method and the MOKE analysis method. This is followed by comparison of the results to other studies and a discussion of the possible relationship between the anisotropy and the atomic structure.

## II. EXPERIMENT

The Fe films were grown on a Cu(001) single crystal in an UHV experimental station where structural characterization of the films is done with medium-energy ion scattering (MEIS) and the magnetic characterization is done using MOKE in the polar geometry. The instrument is described more completely elsewhere.[13] The Cu(001) crystal was cleaned by cycles of Ne sputtering (1700 eV, 1 $\mu$A, 300 K) and annealing to 1000 K. The surface contamination of the Cu and the Fe was checked by x-ray photoemission which showed that there was less than 1% atomic of C or O, the only contaminants observed. The Fe was deposited at $\sim 1$ ML/min from an *e*-beam heated Fe source and the coverage was determined by a quartz crystal monitor which was calibrated by MEIS for coverages between 1 and 3 ML. The absolute accuracy of the 3 ML determination is $\pm 0.2$ ML, with higher coverages having $\pm 10\%$ uncertainty. Fe films were grown at 100 K and at RT. The 100 K grown films were usually annealed to RT briefly before taking either MOKE or MEIS measurements, although some unannealed samples were examined. All MOKE and MEIS measurements were taken with the Fe films at 100 K. The glide-distorted fcc and bcc Fe films have Curie temperatures above RT. Thus, $M_s$ values for these films should be close to $M_s$ at zero temperature. The MOKE apparatus, using 633 nm light, allows hysteresis loops to be taken in two polar geometries. The first of these is the standard polar setup, where the sample normal is aligned with the axis of the applied field. This geometry was used to obtain the Kerr ellipticity at magnetic saturation when the easy axis is either perpendicular to the film or in the film plane. Saturation in the latter case is achieved by applying a large enough $H$ to rotate the magnetic moment from in-plane to perpendicular. The largest value of $H$ needed to rotate the moment is of the order of $4\pi M_s$, which for bcc Fe at 100 K is 2.2 T and is within the range of the insitu 3 T superconducting, split coil solenoid. The value of $H$ at the point where the moment is saturated along the hard axis for the case of the easy axis being in plane, $\alpha = 90°$, is equal to $H_{\text{eff}}$ when $K_2$ is small. With $H$ normal to the film any anisotropy between crystal directions within the film plane is undetected by this method. At the same time it will not affect the results presented here. In the second polar geometry the sample normal is rotated by $\sim 65°$ with respect to the field axis of the solenoid, $\alpha = 65°$. The Kerr optics are set up for near normal incidence and reflection, so that at low applied fields the normal square hysteresis loop is measured,

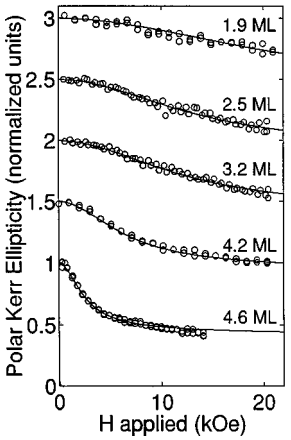


FIG. 1. Raw polar Kerr ellipticity data for Fe films of the indicated coverages for the Kerr setup with the angle between $H$ and the sample normal at $\sim 65°$. The normalized data (shifted for clarity) show the reduction of the Kerr signal as the non-normal applied field causes the moment to rotate away from the film's normal. The solid curves are best fits to the data assuming a uniaxial anisotropy model and with the second-order and higher components set to zero.

for the case of the easy axis perpendicular to the film. As $H$ is increased to higher field values the uniaxial moment rotates toward the field axis and the Kerr ellipticity is reduced from the saturation value by the $\cos\theta$. This reduction in the Kerr ellipticity with increasing $H$ following saturation is shown in Fig. 1 for several Fe coverages for 100 K (annealed) growth. Note that the data are vertically shifted in Fig. 1 for clarity and the plotted changes in ellipticity versus $H$ are normalized to 1.0 in each case. Following standard analysis of Eqs. (1)–(3) for $\alpha = 65°$,[14] $H_{\text{eff}}$ for films with perpendicular easy axis is obtained. The lines through the Kerr ellipticity data are the best-fit results from this analysis when $K_2$ in Eq. (1) is assumed zero. Analysis was done including a nonzero $K_2$ as a parameter. At low coverage (see upper data in Fig. 1), the uncertainties in the raw data do not allow meaningful determinations of these anisotropy terms. At Fe coverages near the spin reorientation, the value of the second-order anisotropy field was $<15\%$ of $H_{\text{eff}}$. We only report results for $K_2$ assumed to be zero. Note that when $H_{\text{eff}} < 0$, the easy axis is perpendicular to the film and when $H_{\text{eff}} > 0$, there is an in-plane easy axis. From Eq. (2) $H_{\text{eff}}$ can only be negative when $K_v$ and/or $K_s$ are positive, i.e., perpendicular anisotropy constants.

## III. RESULTS AND DISCUSSION

### A. Growth at 100 K

The values of $H_{\text{eff}}$ determined using the above methods, as a function of Fe coverage are presented in Fig. 2. There are two distinct regions corresponding to dramatically different magnetic anisotropies. The region where $H_{\text{eff}}$ varies more slowly with 1/(Fe thickness) is the coverage range where the atomic structure is known to be glide-distorted fcc Fe. The more rapidly varying region correlates with the presence of bcc Fe. The vertical dashed line near 1/(Fe thickness) of 0.29 indicates the Fe coverage where MEIS blocking curves begin

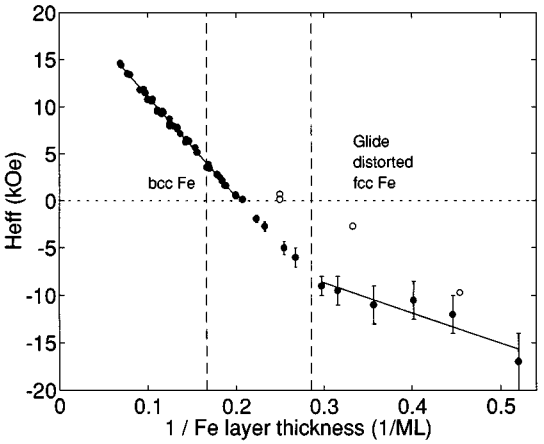


FIG. 2. Plot of $H_{\text{eff}}$ vs 1/(Fe thickness) for Fe films grown on Cu(100) at 100 K and annealed to RT (solid circles). The lines are least-squares linear fits to the data in two regions. The open circles are for Fe films prior to annealing. The dashed vertical lines mark the onset and completion of the fcc-to-bcc transformation.

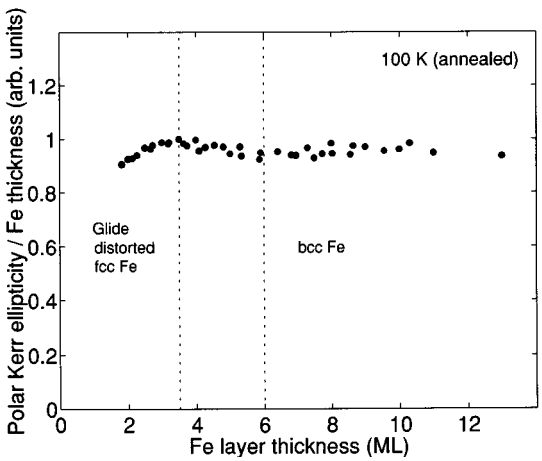


FIG. 3. Plot of the relative polar Kerr ellipticity at magnetic saturation normalized by the Fe film thickness as a function of the Fe film thickness for Fe films grown at 100 K and annealed to RT. The dashed vertical lines mark the onset and completion of the fcc-to-bcc transformation.

to show structural changes due to the initiation of the fcc-to-bcc phase change. The dashed vertical line at 0.16 indicates the coverage where the phase change to bcc Fe is complete. There is a marked change in the slope of $H_{\text{eff}}$ versus 1/(Fe thickness) at the onset of the fcc-to-bcc phase change, indicating a large change in the thickness-dependent component of anisotropy. The changes in the intercepts of the linear segments indicate large changes in the thickness-independent component of anisotropy. As the phase change continues to completion there are additional small changes in the anisotropy. The most likely explanation for this is a significant, almost abrupt, change in the overall strain state and/or the elastic properties of the film at the beginning of the transformation. This abrupt behavior suggests that the phase change does not start or nucleate in localized regions, but proceeds simultaneously throughout the entire film with an extension and reorganization of the glide distortion of the fcc lattice into the new bcc lattice. During the transformation the film has transitional structures which have magnetic anisotropy similar to the final bcc Fe structural phase. In contrast to this inferred behavior for the 100 K Fe growth, scanning tunneling microscopy (STM) results[7,15] and our Kerr results indicate that the fcc-to-bcc phase transformation for RT growth proceeds via the nucleation of bcc regions which grow with increasing Fe coverage. Note that the crossover from a perpendicular to an in-plane easy axis takes place after the anisotropy constants of the film have already changed to those for the bcc film.

Since linear segments are apparent for both structural phases a slope and an intercept can be determined, where the slope is related to $K_s$ and the intercept to $K_v$ through Eqs. (2) and (3). Values of the slopes and intercepts are given in Table I. In order to derive $K_s$ and $K_v$ from these values, an estimate of $M_s$ must be obtained for these films. Figure 3 shows the polar MOKE ellipticity signal at magnetic saturation normalized by the Fe thickness plotted versus the Fe thickness. Due to the use of a single MOKE geometry over the entire coverage range, the glide-distorted fcc Fe film Kerr signal can be directly compared to the bcc Fe film signals, independent of the magnetic easy axis. By 14 ML Fe, the Fe film is expected to have nearly the bulk Fe magnetic moment.[16] As seen in Fig. 3, the variation of the Kerr signal with the Fe thickness is less than $\pm 5\%$ of the average over the range examined. While the Kerr signal is proportional to the magnetic moment, the proportionality is also effected by the atomic structure and the film thickness through subtle changes in the electronic structure. Although not known in detail, simple modeling using bcc Fe optical constants suggests that the film thickness does not alter the proportionality below 15 ML. The effect of the phase transformation on the proportionality is not as clear. However, an assumption that the magnetic moment is approximately constant at all coverages from 2 ML to 14 ML and equal to 1737 $e$mu/cm$^3$, the bulk bcc Fe moment, should be accurate enough for the present discussion, given the uncertainties in determining $H_{\text{eff}}$. An error by as much as 30% in $M_s$ does not affect the basic conclusions of this paper.

Estimates of $K_v$ and $K_s$ for both the bcc Fe films and the glide-distorted fcc Fe films are given in Table I. The values

TABLE I. Anisotropy results for Fe on Cu(100) grown at 100 K and annealed to RT.

| | $(4\pi M_s - 2K_v/M_s)$ (kOe) | $K_v$ (ergs/cm$^3$) | $4K_s/M_s$ (kOe cm) | $K_s$ (ergs/cm$^2$) |
|---|---|---|---|---|
| Glide distorted fcc Fe on Cu(001) | $0.7 \pm 5$ | $1.8 \pm 0.6 \times 10^7$ | $6.0 \pm 2 \times 10^{-4}$ | $0.26 \pm 0.09$ |
| bcc Fe(110) on Cu(100) | $21.7 \pm 0.2$ | $1 \pm 3 \times 10^5$ | $21.6 \pm 0.6 \times 10^{-4}$ | $0.94 \pm 0.14$ |
| Bulk bcc Fe(001) (Ref. 17) | | $5.5 \times 10^5$ | | |

of $K_v$ can be compared to the bulk value for Fe of $5.5\times10^5$ ergs/cm$^3$.[17] $K_v$ for the bcc Fe film is smaller at $1\times10^5$ ergs/cm$^3$ and is directed along the film normal, $\langle 110\rangle$, rather than a $\langle 100\rangle$ direction as in the bulk, which may indicate some residual strain in the bcc film. However, the thickness-independent anisotropy, in this case, is dominated by the large shape anisotropy which makes the uncertainty in $K_v$ so large that the direction of this anisotropy is uncertain. In either case, this term contributes very little to the total anisotropy energy. For the glide-distorted fcc Fe $K_v=1.8\times10^7$ ergs/cm$^3$, which is more than 30 times larger than for bulk bcc Fe. This is an extremely large value for $K_v$ and contributes a perpendicular anisotropy unlike $K_v$ in bulk bcc Fe. This anisotropy must be magnetoelastic in origin and related to strain caused by the $\sim6\%$ expansion of the fcc Fe layers normal to the Fe film and the shear of the associated glide distortion. Magnetoelastic constants for fcc Fe are now known, as fcc Fe is not normally ferromagnetic. Thus, a prediction of the strain-induced anisotropy based on fcc Fe cannot currently be made. Nevertheless, for the sake of comparison, a coarse estimate of the magnetoelastic anisotropy constant for bcc Fe for an average 6% normal strain gives $1.8\times10^6$ ergs/cm$^3$ according to

$$K_v^{\epsilon}=\frac{3}{2}\lambda_{100}(c_{11}-c_{12})\epsilon, \tag{4}$$

as defined by Chikazumi,[18] where $\lambda_{100}$ is a magnetoelastic constant for bcc Fe, $c_{11}$ and $c_{12}$ are elastic stiffness constants for bcc Fe, and $\epsilon$ is the normal strain. This estimate of $K_v^{\epsilon}$ is a factor of 10 smaller than the measured value for the glide-distorted fcc Fe. Equation (4) neglects any effect of the in-plane shear strain on the perpendicular anisotropy, and this would be important if the in-plane magnetoelastic constant is negative.[18] Obviously, larger values for $\lambda_{100}$ and/or $c_{11}-c_{12}$ would help negate the discrepancy. Actually, there is evidence from extended x-ray-absorption fine-structure (EXAFS) measurements of Magnan *et al.*[8] that there are greatly enhanced elastic constants for glide-distorted fcc Fe relative to undistorted fcc Fe. They infer large interlayer force constants for 3.5 ML Fe on Cu(001) at RT based on the very small variation of the Debye-Waller factor with changing film temperature. Our 100 K (annealed) grown Fe films have a very similar structure to the RT grown films at this coverage.[4] Thus, the extraordinarily high value for $K_v$ found here could have its origin in and is in qualitative agreement with the large interlayer force constants found by EXAFS. Unfortunately, phonon dispersion curves obtained by Daum *et al.*[19] for Fe films on Cu(001) are not really consistent with large interlayer force constants, however their Fe coverage was miscalibrated making the reported coverage low by a factor of 2–3, which may, if properly accounted for, clear up the discrepancy with the EXAFS result. Neither of these prior studies accounted for the $(5\times1)$ glide distortion in their analyses, which could also impact their data interpretations.

The phase transformation from fcc-to-bcc reduces $K_v$ by a factor of $>100$. This large reduction is apparently coupled to the release of Fe lattice strain during formation of the new bcc lattice, according to the structural evidence. This is consistent with MEIS measurements which show considerable atomic disorder in the Cu substrate and which, therefore, suggest that much of the Fe/Cu interfacial strain resides in the Cu.[4]

The thickness-dependent anisotropy constants given in Table I are averages for the interfaces, Cu/Fe and Fe/vacuum, and for any volume contribution to the thickness dependence. The phase transformation from fcc-to-bcc causes $K_s$ to increase by a factor of 3.6. Associated with the phase transformation is an increase in the Fe in-plane areal density of about 9% and a 5% increase in layer spacing throughout the film. There are bcc Fe domains with four different orientations on the Cu fcc substrate,[7] and the Fe is nonpseudomorphic with the Cu. Additionally, the roughness of the Cu/Fe interface increases as reflected by an increase in the MEIS ion scattering yield from Cu following the phase transformation,[4] however there is negligible interdiffusion for 100 K growth of Fe. The surface topography of the Fe cannot be examined by MEIS, but STM studies show that the bcc Fe becomes rough during growth.[20] Even though such structural changes must be the origin of the increase in $K_s$, neither first-principles theoretical calculations of magnetic anisotropy[21] nor phenomenological theories of anisotropy[22,23] provide an explanation of why $K_s$ behaves as it does in this particular case.

The value of $K_s$ for the fcc Fe phase is about a factor of 2 lower than previously reported FMR measurements for Cu/Fe/Cu sandwiches.[24] This difference may be partially attributed to the Fe film having two Fe/Cu interfaces in the previous study, whereas there is one each, Fe/Cu and Fe/vacuum, in the present study. On the other hand, the origin for this discrepancy could be the different treatment of $K_v$. In previous work, $K_v$ was assumed small compared to $K_s$ and it was neglected. As discussed above, $K_v$ for the glide-distorted fcc Fe actually contributes more to the perpendicular anisotropy than does $K_s$ at all thicknesses in the uncapped film, when the fcc Fe film is ferromagnetic. If the glide reconstruction were removed when the Fe layer is sandwiched between the Cu as indicated by EXAFS,[8] then the anisotropy of the sandwich structure would be different from the uncapped Fe layer. However, other sandwich studies provide fairly strong, although indirect, magnetic evidence that the Fe reconstruction must still be present in sandwich structures, since high spin moments are found.[25,26] High spin moments are observed to coincide with the increased atomic volume of the glide-distorted fcc Fe. We conclude that the previous value of 0.63 ergs/cm$^2$ for $K_s$ for the fcc Fe/Cu interface is too high by as much as a factor of 2, with the exact amount dependent on the extent of the glide-distortion–expansion found in the capped Fe films.

For the bcc Fe(011) film on Cu we derive $K_s=0.94$ ergs/cm$^2$ from the slope of the data in Fig. 2. A value of 0.96 ergs/cm$^2$ has been found for the bcc Fe(001)/vacuum interface[28] and a value of 0.8 ergs/cm$^2$ was obtained for the bcc Fe(001)/Ag interface.[27,28] The mean of these latter two values, 0.88 ergs/cm$^2$, is the appropriate value to compare to our measured value. Thus, to within our estimated errors these interface anisotropy values are the same. Since the electronic structure of Cu(001) and Ag(001) are rather similar, the Fe/substrate electronic overlap should also be similar making direct comparison of the anisotropies reasonable. Additional evidence for this is that the calculated magnetic

moment of an Fe monolayer on either substrate is the same.[16] A simple linear theory of anisotropy which compares orientation dependences[29] indicates that for unstrained layers the interface anisotropy for a bcc(011) interface should be about 30% smaller than for a bcc(001) interface. Within the present assumptions, one concludes that the equivalence of the interface anisotropy of bcc Fe(011) on Cu compared to bcc Fe(001) on Ag is likely due to residual strain at the bcc/fcc interface of one or both of these Fe/metal couples.

The spin reorientation from perpendicular anisotropy to in-plane anisotropy is quite striking and has previously been attributed directly to the iron structural phase transition.[5] This is incorrect, as is readily seen in Fig. 2, where the magnetic anisotropy constants are observed to change to their new values at a lower Fe thickness, at the onset of the transformation. The reorientation is actually just the result of the perpendicular thickness-dependent anisotropy being overwhelmed by the shape anisotropy as the Fe coverage increases. It is only connected to the formation of the bcc phase in as much as $K_s$ and $M_s$ for the bcc film are the important quantities defining the exact Fe thickness for the reorientation. The Fe coverage, 4.8 ML, where this occurs is in good agreement with some other studies of Fe on Cu,[5,30] showing that the Fe thickness calibration is comparable between these studies. Additionally, this coverage is in the range of Fe coverages reported for the spin reorientation for bcc Fe on Ag(100).[31–33] This is to be expected in view of the similar moments of bcc Fe on Cu and on Ag, the nearly bulk value of $K_v$, and the similarity of $K_s$ between bcc Fe on Cu or on Ag, as discussed above.

Figure 2 includes a few $H_{\text{eff}}$ values for 100 K grown Fe films which are unannealed. $H_{\text{eff}}$ of the 4 ML film shows that it has in-plane anisotropy before it is annealed. Even though the data are very limited, an estimate of the anisotropy constants can be made giving $K_v = 4\times10^6$ ergs/cm$^3$ and $K_s = 0.3$ ergs/cm$^2$. These values are intermediate to those in Table I for the bcc Fe and the glide-distorted fcc Fe. The reduction of $K_v$ from the glide-distorted fcc Fe value weakens the perpendicular anisotropy considerably, as already indicated by the observed spin reorientation at 4 ML. $K_s$ is nearly the same as the value for the fcc Fe. The similarity of $K_s$ before and after the anneal is not too surprising since the local atomic arrangement is mostly fcc-like in both cases, although by 4 ML some bcc Fe is present. The two MEIS blocking curves in Fig. 4 for the 3 ML Fe film are a comparison of the local atomic structure before and after the RT anneal. After the anneal, the structure described in Refs. 2 and 4 is fully formed, where the lattice coherency is of the order of 20 atoms across.[34] Prior to the anneal, the blocking minima at 35°, 38°, 46°, and 53° are less deep. This indicates that the local atomic order is less in the unannealed film, as might be expected, and the complete loss of the blocking minima at 35° (⟨701⟩ direction) indicates that there is a loss of lattice coherency within the Fe for fourth nearest neighbors and beyond. The blocking minima present prior to the anneal have nearly the same scattering angles as compared to after the anneal indicating that the glide-distortion–layer-expansion is partially formed during the cold growth prior to the anneal. This is consistent with the MOKE measurements which show a strong ferromagnetic signal before annealing, although it is reduced by about 15% compared to post-anneal. Current understanding of the relationship between the Fe moment and the local atomic structure requires a larger atomic Fe volume compared to perfect fcc Fe to achieve high spin, ferromagnetic coupling, as is observed. The glide-distortion–layer-expansion results in a large atomic volume and thus its presence before the anneal assures a ferromagnetic Fe film. The value of $K_v = 4\times10^6$ ergs/cm$^3$ for the unannealed film is qualitatively self-consistent with a partially formed internal strain, since it is substantially larger than the value for the nearly unstrained bcc Fe, but is about five times lower than that of the fully strained, annealed film.

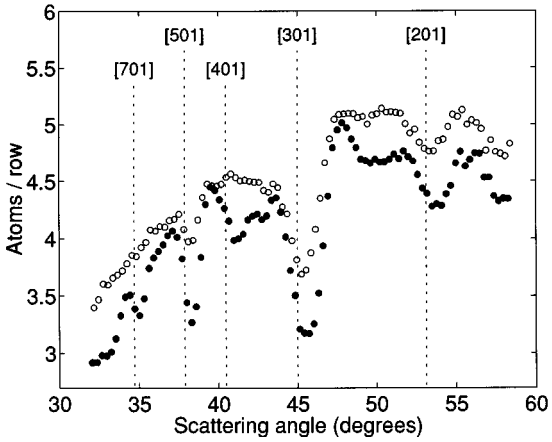


FIG. 4. MEIS blocking curve for 200 keV $H$ incident along the ⟨201⟩ direction for the scattering angles shown for a 3 ML Fe film grown on Cu(100) at 100 K prior to (open circles) and following (solid circles) a brief RT anneal.

### B. Growth at RT

The $H_{\text{eff}}$ values for RT Fe growth are plotted in Fig. 5 versus 1/(Fe thickness). The two dashed vertical lines between 0.2 and 0.3 mark the transition region between the two fcc structures according to when the Kerr ellipticity at magnetic saturation begins to fall off with increasing Fe thick-

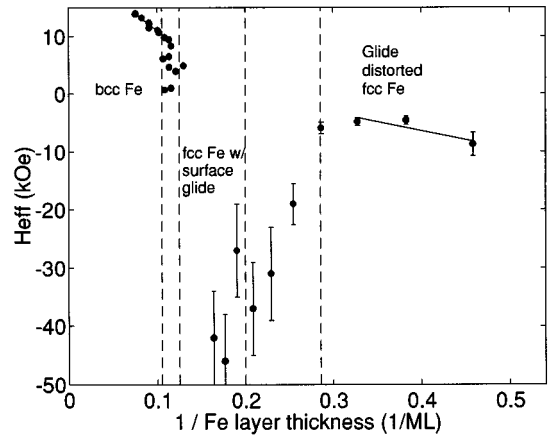


FIG. 5. Plot of $H_{\text{eff}}$ vs 1/(Fe thickness) for Fe films grown on Cu(100) at RT. The lines are least-squares linear fits to the data in two regions. The dashed vertical lines mark the onset and completion for the fcc-to-bcc transformation and the glide-distorted fcc-to-fcc with surface reconstruction transformation.

ness and then plateaus.[4] The two dashed vertical lines just above 0.1 mark the range of Fe coverage during which the fcc-to-bcc phase transition takes place as indicated by a rapid increase of the Kerr signal with increasing Fe coverage from the plateau of low Kerr signal. The lack of extended linear regions in $H_{\text{eff}}$ versus 1/(Fe thickness) due to the presence of an antiferromagnetic fcc phase at intermediate thickness makes determination of $K_v$ and $K_s$ more difficult. In addition, there is limited RT data at low Fe coverages. Within these limitations we find that the glide-distorted fcc Fe has $K_v = 1.4 \times 10^7$ ergs/cm$^3$ and $K_s = 0.3$ ergs/cm$^2$. The anisotropy constants are the same as for 100 K (annealed) growth, to within the experimental and analytical uncertainties. The bcc Fe has $K_s = 1.0$ ergs/cm$^2$, the same as the 100 K (annealed) grown bcc Fe films. An estimate for $K_v$ is $-1 \times 10^6$ ergs/cm$^3$, which is an in-plane anisotropy and nearly twice the bulk bcc Fe value. Very little can be said about the anisotropy constants in the intermediate fcc Fe region. Since the fcc Fe bulk is antiferromagnetic,[35] the ferromagnetic Kerr signal is generally thought to be due to ferromagnetic coupling at the surface associated with the surface glide reconstruction at these Fe coverages. In passing, it is interesting to note that if $H_{\text{eff}}$ versus 1/(Fe thickness) data for the glide-distorted fcc Fe in Fig. 2 is extrapolated to lower coverage, the $H_{\text{eff}}$ values are comparable to those for the fcc RT Fe films of 5–6 ML when the extrapolated coverage is of the order of 1 ML. Additionally, the magnitude of the glide distortion and layer expansion of the surface reconstruction, although having a different in-plane periodicity, is the same as has been determined for each layer of the glide-distorted fcc Fe.[4] This is reasonably consistent with the Kerr ellipticity signal observed from Fe films with this surface reconstructed fcc phase, which is 1.2–1.7 times the signal expected from a single ferromagnetic layer having the bulk bcc Fe moment.[2,6,4] These observations indicate that the ferromagnetic region in this intermediate fcc phase is roughly 1 ML thick. It is still not entirely clear whether or not there is some ferromagnetic coupling at the Fe/Cu interface in addition to the ferromagnetism at the Fe surface.

The spin reorientation for RT grown Fe films is coincident with the phase transformation of the fcc Fe with the surface-glide reconstruction[1,3] to bcc, which initiates at $\sim 7.5$ ML and is completed by 9.5 ML in the present study. The MOKE hysteresis loops show a mixed character with two identifiable components in this coverage range. One is a square loop of low Kerr ellipticity with a perpendicular easy axis, just as is observed or the pure fcc Fe with the surface-glide reconstruction. The second component has an in-plane easy axis and a much larger Kerr signal at saturation characteristic of pure bcc Fe. Thus, during the transition there are regions of the film that are fully bcc Fe and other regions which are still fcc Fe, as opposed to the entire film going through a continuous, gradual transformation. At the end of the transformation the bcc Fe film has an in-plane easy axis because the thickness of magnetic Fe is greater than the spin reorientation thickness for bcc Fe, $\sim 5$ ML, at the point where a region goes bcc. Note that if the phase change had only caused the observed changes in the anisotropy constants, but had not caused a change in the magnetic thickness, then the Fe film would still have had a perpendicular easy axis. Thus, it is the abrupt increase in magnetic thickness upon formation of bcc Fe that drives the reorientation to an in-plane easy axis.

Hembree *et al.*[36] have reported a metastable magnetic field-induced spin reorientation of a 3.5 ML RT Fe film. We have applied 1.1 T perpendicular fields to RT grown films of 2 ML to 4 ML at RT and up to 2.5 T at 100 K and have never observed a spin reorientation, although small variations in the coercivity were observed. The anisotropy must be rather weak for these films at RT, since the Curie temperature is declining with coverage and very near RT for this Fe coverage range and growth conditions. It would not be too surprising if some other factor, such as contamination or substrate irregularities, caused the films to be nearly isotropic in the previous study which might have made them susceptible to small perturbations induced by external fields.

## IV. SUMMARY

Measurements of $H_{\text{eff}}$ for glide-distorted fcc Fe and bcc Fe on Cu(001) have been used to make estimates of the anisotropy constants, $K_v$ and $K_s$, for these magnetic films. In the case of the glide-distorted fcc Fe, the value of $K_v$ is unexpectedly large, and, to date, magnetocrystalline and magnetoelastic models do not provide a full explanation for such a large thickness-independent anisotropy constant. There are indications that the elastic constants of the glide-distorted fcc Fe are unusual which would help explain the huge value of $K_v$. In any case, the glide-distortion–layer-expansion clearly plays an important role in determining the magnitude of the anisotropy. When the Fe film transforms to bcc Fe, $K_v$ reduces to values close to unstrained, bulk bcc Fe. The large, perpendicular value of $K_v$ combined with a perpendicular value for $K_s$ cause the magnetic easy axis of the glide-distorted fcc Fe to be perpendicular. Without the contribution of $K_v$, this film would have an in-plane easy axis. Since $K_v$ is too large to neglect, previous determinations of $K_s$ for these ultrathin fcc Fe films, where $K_v$ was assumed zero, are incorrect. The value of $K_s$ for the glide-distorted fcc Fe, determined here, is 3–4 times smaller than the value found for bcc Fe on Cu(001) and should be related to structural differences between fcc Fe and bcc Fe, although other factors make the exact role difficult to clarify. The observed spin reorientation is nearly, but not quite, coincident with the fcc-to-bcc phase transformation and has therefore been associated, erroneously, with changes in the anisotropy constants, in the past. Although the anisotropy energy and easy axis direction are strongly influenced by the atomic structure, the actual act of reorientation of the spin is triggered by the increased dominance of the shape anisotropy as the ferromagnetic thickness increases either through Fe growth or through the abrupt change in magnetic thickness during the fcc-to-bcc phase change.

The magnetic anisotropy of ultrathin films is an important property and it is being exploited in the development of new magnetic devices and sensors. It is determined by the underlying anisotropies in the atomic structure of the film, which include intrinsic magnetocrystalline anisotropy, extrinsic chemical ordering and alloying, and extrinsic magnetoelastic anisotropy through the presence of strain due to epitaxy and to formation of defects and atomic reconstructions. Each of these structural aspects can make an important contribution

to the overall anisotropy. This is especially true for thin film structures containing Fe layers since Fe shows such a wide variety of behavior, as demonstrated in the present study. It is well known that we are currently still a long way from having first-principles theories that quantitatively explain the experimental situation. In view of the complex experimental observations and of the state of theory, one clearly still needs to experimentally determine the anisotropy constants for each interesting combination of layers of a set of materials in order to make full use of such thin film structures in technological applications.

## ACKNOWLEDGMENTS

J.V.B. wishes to acknowledge the support of the Alexander von Humboldt-Stiftung during this work. We thank C. Chappert for use of his computer program to calculate $H_{\text{eff}}$ from the Kerr hysteresis loops and D. Weller and M. Wuttig for enlightening discussions.

[1] P. Bayer, S. Müller, P. Schmailzl, and K. Heinz, Phys. Rev. B **48**, 17 611 (1993).
[2] S. Müller, P. Bayer, C. Reischl, K. Heinz, B. Feldmann, H. Zillgen, and M. Wuttig, Phys. Rev. Lett. **74**, 765 (1995); K. Heinz, S. Müller, and P. Bayer, Surf. Sci. **337**, 215 (1995).
[3] J. V. Barth and D. E. Fowler, Phys. Rev. B **52**, 1528 (1995).
[4] J. V. Barth and D. E. Fowler, Phys. Rev. B **52**, 11 432 (1995).
[5] H. Zillgen, B. Feldmann, and M. Wuttig, Surf. Sci. **321**, 32 (1994).
[6] J. Thomassen, F. May, B. Feldmann, M. Wuttig, and H. Ibach, Phys. Rev. Lett. **69**, 3831 (1992).
[7] K. Kalki, D. D. Chambliss, K. E. Johnson, R. J. Wilson, and S. Chiang, Phys. Rev. B **48**, 18 344 (1993).
[8] H. Magnan, D. Chandesris, B. Villette, O. Heckmann, and J. Lecante, Phys. Rev. Lett. **67**, 859 (1991).
[9] V. L. Moruzzi, P. M. Marcus, and J. Kuebler, Phys. Rev. B **39**, 6957 (1989); G. L. Krasko and G. B. Olson, *ibid.* **40**, 11 536 (1989).
[10] C. Liu, E. R. Moog, and S. D. Bader, Phys. Rev. Lett. **60**, 2422 (1988).
[11] B. Schulz and K. Baberschke, Phys. Rev. B **50**, 13 467 (1994).
[12] C. Chappert and P. Bruno, J. Phys. **64**, 5736 (1988).
[13] D. E. Fowler, M. W. Hart, and J. V. Barth, Vacuum **46**, 1127 (1995).
[14] S. T. Purcell, M. T. Johnson, N. W. E. McGee, W. B. Zeper, and W. Hoving, J. Magn. Magn. Mater. **113**, 257 (1992).
[15] J. Giergiel, J. Kirschner, J. Landgraf, J. Shen, and J. Woltersdorf, Surf. Sci. **310**, 1 (1994).
[16] A. J. Freeman and R. Wu, J. Magn. Magn. Mater. **100**, 497 (1991).
[17] R. M. Bozorth, *Ferromagnetism* (IEEE, New York, 1993).
[18] S. Chikazumi and S. H. Charap, *Physics of Magnetism* (Wiley, New York, 1964).
[19] W. Daum, C. Stuhlmann, and H. Ibach, Phys. Rev. Lett. **60**, 2741 (1988).
[20] J. Giergiel, J. Shen, J. Woltersdorf, A. Kirilyuk, and J. Kirschner, Phys. Rev. B **52**, 8528 (1995).
[21] J. G. Gay and R. Richter, in *Ultrathin Magnetic Structures I*, edited by J. A. C. Bland and B. Heinrich (Springer-Verlag, Berlin, 1994), p. 21.
[22] P. Bruno, J. Appl. Phys. **64**, 3153 (1988).
[23] H. J. G. Draaisma, F. J. A. denBroeder, and W. J. M. deJonge, J. Appl. Phys. **63**, 3479 (1988).
[24] J. F. Cochran, J. M. Rudd, M. From, B. Heinrich, W. Bennett, W. Schwarzacher, and W. F. Egelhoff, Phys. Rev. B **45**, 4676 (1992).
[25] S. S. P. Parkin and J. Stohr (private communication).
[26] W. R. Bennett, W. Schwarzacher, and W. F. Egelhoff, Phys. Rev. Lett. **65**, 3169 (1990); W. Schwarzacher, W. Allison, R. F. Willis, J. Penfold, R. C. Ward, I. Jacob, and W. F. Egelhoff, Solid State Commun. **71**, 563 (1989).
[27] K. B. Urquhart, B. Heinrich, J. F. Cochran, A. S. Arrott, and K. Myrtle, J. Appl. Phys. **64**, 5334 (1988).
[28] B. Heinrich, Z. Celinski, J. F. Cochran, A. S. Arrott, and K. Myrtle, J. Appl. Phys. **70**, 5769 (1991).
[29] R. H. Victora and J. M. MacLaren, J. Appl. Phys. **73**, 6415 (1993).
[30] R. Allenspach and A. Bischof, Phys. Rev. Lett. **69**, 3385 (1992).
[31] M. Stampanoni, A. Vaterlaus, M. Aeschlimann, and F. Meier, Phys. Rev. Lett. **59**, 2483 (1987).
[32] D. P. Pappas, C. R. Brundle, and H. Hopster, Phys. Rev. B **45**, 8169 (1992).
[33] Z. Q. Qin, J. Pearson, and S. D. Bader, Phys. Rev. Lett. **70**, 1006 (1993).
[34] G. L. Nyberg, M. T. Kief, and W. F. Egelhoff, Phys. Rev. B **48**, 14 509 (1993).
[35] R. D. Ellerbrock, A. Fuest, A. Schatz, W. Keune, and R. A. Brand, Phys. Rev. Lett. **74**, 3053 (1995).
[36] G. G. Hembree, J. Drucker, S. D. Healy, K. R. Heim, Z. J. Yang, and M. R. Scheifein, Appl. Phys. Lett. **64**, 1036 (1994).